INTERNATIONAL JOURNAL FOR NUMERICAL METHODS IN FLUIDS, VOL. 8, 1513–1522 (1988)

A FINITE ELEMENT MODEL FOR THE DISSOLUTION OF CORROSION PITS IN THE PRESENCE OF FLUID FLOW

JOHN N. HARB AND RICHARD C. ALKIRE

Department of Chemical Engineering and Materials Research Laboratory, University of Illinois, Urbana, IL 61801, U.S.A.

SUMMARY

Simulation of the dissolution of an active corrosion pit in the presence of fluid flow was carried out with the use of finite element techniques. The model included multiple species in solution, reaction equilibria and transport by diffusion, convection and migration. The mathematical model was used to examine the effect of fluid flow on the pitting of nickel in neutral chloride solution. The pit dissolution rate was found to decrease with increasing flow owing to potential field effects. The capabilities demonstrated in this paper represent a significant advancement in the modelling of pitting corrosion phenomena.

KEY WORDS Corrosion pits Fluid flow Finite element techniques

INTRODUCTION

The local environment within active corrosion pits is different to that of the external bulk solution owing to transport and reaction phenomena which lead to accumulation or depletion of species inside the pit. Fluid flow can influence pitting corrosion by altering the local composition within the pit. Characterization of the local pit electrolyte is essential to an understanding of pitting, since it is the local environment which determines the growth rate and stability of the pit. The objective of the present study was to develop a mathematical model to simulate conditions within an active corrosion pit and provide a vehicle for quantitative testing of mechanistic hypotheses.

THEORETICAL MODEL

The corrosion pit under consideration is an axisymmetric dissolving cavity on a metal surface which, except for the cavity, is flat and in a passive or non-reactive state. The metal is at constant potential with respect to a reference point far away from the surface. The cavity dissolves as metal ions are transferred from the solid phase to the aqueous solution, resulting in a local increase in concentration of positively charged metal ions. There is a simultaneous build-up of negatively charged ions inside the cavity in order to balance the electrical charge. The metal ions are transported out of the pit interior by diffusion, migration and convection. They may also react with other ions in solution to form additional species. These reactions are usually fast and are considered to be in equilibrium. The dissolving cavity is a moving boundary problem which may be considered to be at quasi-steady state owing to the fact that the characteristic time for the boundary movement is greater than the time necessary for the transport processes to reach steady state.

0271–2091/88/121513–10$05.00

Received 7 December 1987
Revised 8 April 1988

The specific system chosen for study was the pitting of nickel in sodium chloride solution at neutral pH. Nickel dissolves into solution as Ni^{+2}.[1] Once in solution, the nickel ion can further react to form chloride complexes according to the following reactions:[2,3]

$$Ni^{+2} + Cl^{-} = NiCl^{+}, \tag{1}$$

$$Ni^{+2} + 2Cl^{-} = NiCl_2. \tag{2}$$

The nickel ion also undergoes hydrolysis. The extent of hydrolysis at neutral pH, however, is not enough to cause precipitation of solid hydrolysis products.[4,5] Hydrolysis products can therefore be neglected because of their very low concentration and the fact that no precipitation occurs.

The species included in the model are numbered for convenience as shown below:

1	$NiCl^{+}$	4	Cl^{-}
2	$NiCl_2$	5	Na^{+}
3	Ni^{+2}	6	ϕ.

Species 6 is the electrostatic potential whose gradient is the negative of the electric field. The partial differential equations resulting from the individual species balances are

$$-\nabla \cdot N_1 - \nabla \cdot N_2 - \nabla \cdot N_3 = 0, \tag{3}$$

$$-\nabla \cdot N_1 - 2\nabla \cdot N_2 - \nabla \cdot N_4 = 0, \tag{4}$$

$$-\nabla \cdot N_5 = 0, \tag{5}$$

where N_i is the flux of species i defined as

$$N_i = -D_i \nabla c_i - z_i F u_i c_i \nabla \phi + \mathbf{v} c_i. \tag{6}$$

The three terms in the flux equation represent transport by diffusion, migration and convection respectively. The migration term, unique to electrochemical systems, describes the movement of charged species in response to the electric field. Only solvent (water)–ion interactions are considered. Physical parameters were assumed to be constant. Species continuity equations for the hydrogen and hydroxide ions were not included, since these two species are essentially decoupled from the rest of the species in solution owing to their very low concentration. Equations (3) and (4) are balances on species containing Ni and Cl respectively and were obtained by eliminating the reaction rate terms from the individual species balance equations. The reaction equilibria expressed in equations (1) and (2) provide two additional relations:

$$K_1 = c_1 / c_3 c_4, \tag{7}$$

$$K_2 = c_2 / c_3 c_4^2. \tag{8}$$

The set of equations is closed with the electroneutrality equation

$$\sum_i z_i c_i = 0, \tag{9}$$

where z_i is the charge on species i. Equation (9) is an implicit equation for the electrostatic potential which requires that the net charge of the solution be equal to zero.

The domain of interest is shown in Figure 1. Distances have been normalized with respect to the radius of the cavity opening (r_0). The cavity itself is a spherical section with a characteristic angle of 69° (Figure 1) chosen to approximate the shape of experimentally observed pits in 1 M NaCl.[5]

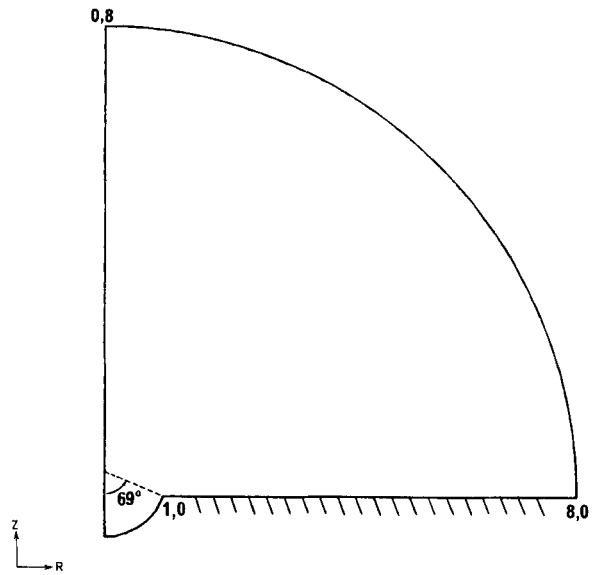

Figure 1. Solution domain for axisymmetric cavity. Distances have been normalized with respect to the radius of the cavity opening

The left boundary is the axis of symmetry at which the following conditions apply:

$$N_1 \cdot \mathbf{n} + N_2 \cdot \mathbf{n} + N_3 \cdot \mathbf{n} = 0, \tag{10}$$

$$N_1 \cdot \mathbf{n} + 2N_2 \cdot \mathbf{n} + N_4 \cdot \mathbf{n} = 0, \tag{11}$$

$$N_5 \cdot \mathbf{n} = 0. \tag{12}$$

These same boundary conditions also apply at the lower boundary (excluding the cavity surface). Conditions (11) and (12) are valid at the cavity surface, where condition (10) is replaced by

$$N_1 \cdot \mathbf{n} + N_2 \cdot \mathbf{n} + N_3 \cdot \mathbf{n} = \frac{i_0}{2F} \exp\left[\beta(\phi_m - \phi)\right]. \tag{13}$$

The exponential expression describes the dissolution of nickel as a function of the potential and is commonly referred to as a Tafel relation. The boundary conditions at the outside boundary are

$$\begin{aligned} c_1 = c_2 = c_3 = 0, \qquad & c_4 = c_{4,\,\text{bulk}}, \\ \phi = 0, \qquad & c_5 = c_{5,\,\text{bulk}}. \end{aligned} \tag{14}$$

In other words, the concentrations at the outside boundary were set equal to bulk conditions. The outside boundary was placed a sufficient distance from the cavity so as not to distort the concentration profiles in the cavity region (within five radii of the cavity centre). An additional correction was necessary for the electrical potential. The potential drop from the outside boundary to infinity was significant and was accounted for by use of an analytical expression. The reason for the round shape of the outside boundary was to approximate the shape of a constant potential line. The absolute value of the potential is arbitrary and was set equal to zero at the outside boundary. The equilibrium relations and the electroneutrality equation apply at all boundaries.

The above equations and boundary conditions which describe the concentration and potential fields were made dimensionless prior to numerical solution (see Reference 5). An important parameter which appears in the dimensionless equations is the Peclet number defined as

$$Pe = u_0 r_0 / D_1. \tag{15}$$

In physical terms the Peclet number is the ratio of convective transport to transport by diffusion.[6]

FLUID FLOW

In order to preserve the symmetry of the problem, the cavity was subjected to flow from an axisymmetric jet whose axis was coincident with that of the cavity. The size of the jet was large with respect to the small cavities of interest (radius of cavity opening: 30–40 μm). Viscous forces dominate in the region of interest owing to the small size of the cavities. Therefore, the Stokes equations adequately describe the flow field near the cavity. The equations are independent of the concentration field and may be solved directly to obtain the hydrodynamic field. Because the equations are linear in velocity, the calculated velocity field can be scaled to any velocity for which the Stokes assumption is valid.

The flow equations were also solved in their dimensionless form. The characteristic velocity was that at the top of the domain ($R=0, Z=8$). With respect to Figure 1, the boundary conditions used are

$$\begin{aligned} \partial V_z/\partial \mathbf{n} &= 0 \quad \text{left-hand boundary,} \\ V_z &= 0 \quad \text{lower boundary,} \\ V_z &= V_{hz} \quad \text{outer boundary,} \\ V_r &= 0 \quad \text{left and lower boundaries,} \\ V_r &= V_{hr} \quad \text{outer boundary.} \end{aligned} \tag{16}$$

V_{hr} and V_{hz} were approximated at each point along the outer boundary by expanding the similarity solution for the laminar boundary layer of an infinite axisymmetric jet impinging on a flat plate, and keeping the first non-zero term of the series.[7] The resulting expressions for the velocities near the wall are

$$V_{hr} = ARZ, \qquad V_h = -AZ^2, \tag{17}$$

where A is a constant.

METHOD OF SOLUTION

The FIDAP Analysis Package was used to solve the fluid flow equations.[8] The package uses the Galerkin formulation of the finite element method to solve a variety of fluid dynamics and convective heat transport problems.

In order to solve for the concentration and potential fields, the Galerkin procedure was applied to equations (3)–(5) to yield the discrete equations of the form

$$\sum_i [(\mathbf{H} + \mathbf{G}_i)\mathbf{C}_i] + \left(\sum_i \mathbf{P}_i\right)\boldsymbol{\phi} = \sum_i \mathbf{F}_i, \tag{18}$$

where

$$\mathbf{H}=\int_v \Gamma^{\mathrm{T}}\mathbf{v}\cdot\nabla\Gamma\,\mathrm{dV},$$

$$\mathbf{G}_i=\int_v D_i\nabla\Gamma^{\mathrm{T}}\nabla\Gamma\,\mathrm{d}V,$$

$$\mathbf{P}_i=z_i F\int_v u_i c_i\nabla\Gamma^{\mathrm{T}}\nabla\Gamma\,\mathrm{dV},$$

$$\mathbf{F}_i=\int_s \Gamma^{\mathrm{T}}\left(D_i\frac{\partial c_i}{\partial\mathbf{n}}+z_i F u_i c_i\frac{\partial\phi}{\partial\mathbf{n}}\right)\mathrm{d}S.$$

The summations are over the species included in the particular equation (see equations (3)–(5) above). The discrete forms of the equilibrium relations (7) and (8) are

$$K_3\mathbf{E}\mathbf{C}_1-\mathbf{B}_4\mathbf{C}_3=0,\qquad K_4\mathbf{E}\mathbf{C}_2-\mathbf{B}_4\mathbf{C}_1=0, \tag{19}$$

where

$$\mathbf{E}=\int_v \Gamma^{\mathrm{T}}\Gamma\,\mathrm{d}V,$$

$$\mathbf{B}_i=\int_v c_i\Gamma^{\mathrm{T}}\Gamma\,\mathrm{d}V,$$

$$K_3=1/K_1,\qquad K_4=K_1/K_2.$$

Finally, the electroneutrality equation can be written as

$$\sum_{\text{all } i} z_i\mathbf{E}\mathbf{C}_i=0. \tag{20}$$

The FIDAP code was modified to solve the above set of discrete equations which describe the concentration and potential fields. Additional modifications were required to apply the boundary condition (13). The details of the modifications can be found in Reference 5. A Newton–Raphson iteration procedure was used to solve the highly non-linear system.

Nine-noded quadratic elements of isoparametric form were used in a finite element mesh of 139 quadrilateral elements and 601 nodes. The mesh was designed to optimize the solution of the mass transport problem, since solution of the Stokes equations for the flow field presented no difficulty. All simulations were carried out on an IBM mainframe (3081-GX) using 4 Mbyte virtual memory.

RESULTS AND DISCUSSION

Fluid flow calculations

Figure 2 shows the velocity field where the length of each vector is proportional to the magnitude of the velocity at that point. The flow velocity decreased rapidly as it approached the wall. Velocities in the cavity were approximately five orders of magnitude smaller than those at the top of the domain. Flow field calculations required approximately 11·4 CPU seconds.

It should be noted that the normal velocity was completely specified over the entire boundary of the domain. Under such conditions, the specified boundary conditions must satisfy the discrete

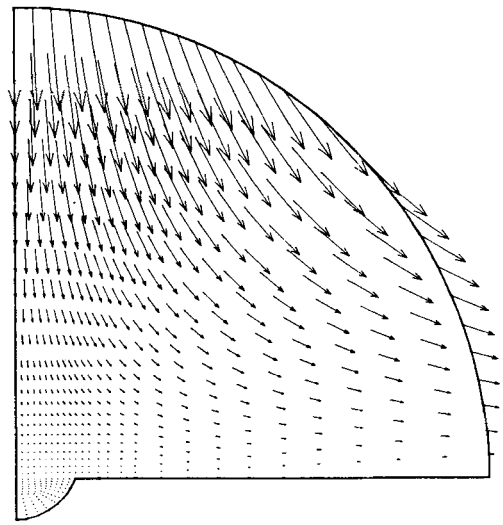

Figure 2. Velocity vector plot for Stokes flow in the cavity region. The vector length is proportional to the magnitude of the velocity at that point

mass balance or the problem is ill-posed, the algebraic system will be inconsistent and no solution is possible.[9] If the global mass balance is satisfied, then the pressure can be determined to an arbitrary additive constant. Apparently the analytical solution (equation (17)) applied at the boundary was interpolated exactly by the quadratic basis functions and thus satisfied the discrete mass balance. This observation is supported by the fact that solution of the flow field both with the use of a penalty method and with discretized pressure gave equivalent answers.

Pitting simulations

Figure 3(a) shows concentration contours for Ni^{+2} resulting from the dissolution of nickel in 1 M NaCl under no-flow conditions. It is evident that the concentration variations extend well beyond the pit mouth. Thus, transport resistance outside the cavity was an important part of the total transport resistance.

The effect of flow on the concentration field is seen in Figures 3(b) and 3(c) which show iso-concentration lines for Ni^{+2} at different flow rates as characterized by Peclet numbers of 10 and 500. An increase in Peclet number corresponds either to an increase in velocity or an increase in the size of the cavity. Fluid flow limited concentration variations to the region close to the lower boundary of the domain. However, no penetration of the mass transfer boundary layer into the cavity was observed. Figure 4 shows the variation of all species from the bottom of the pit outward along the axis of symmetry for a Peclet number of 10. The concentration of Ni species represents the sum of species 1, 2 and 3. The concentrations reached their bulk values within about four radii from the pit mouth. The potential, however, continued to drop slowly throughout the domain. A pitting simulation required approximately 700–1200 s to converge, depending on the particular conditions of the run.

Figure 5 shows the variation of the local dissolution rate (dimensionless) along the surface of the cavity at two values of *Pe* for bulk concentrations of 1·0 M NaCl and 0·25 M NaCl. Dissolution rates for the 0·25 M solution were about 40% lower than for the 1·0 M solution owing to the

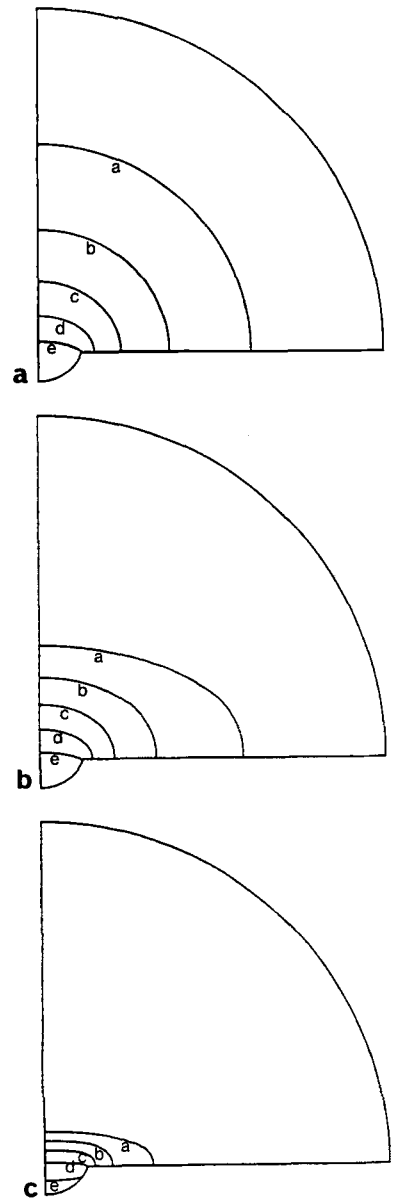

Figure 3. Ni^{+2} iso-concentration lines for nickel dissolution in 1 M NaCl at (a) $Pe=0$ (no flow), (b) $Pe=10$ and (c) $Pe=500$. Contour legend: a, 0·2 M; b, 0·4; c, 0·6; d, 0·8; e, 1·0

higher conductivity of the more concentrated solution. For each bulk concentration the dissolution rate was found to decrease with increasing Peclet number. The decrease was slightly more pronounced for the 0·25 M NaCl solution than for the 1 M NaCl solution. Convective flow caused the electrolyte solution inside the domain (Figure 1) to become more like the bulk solution. Thus, the concentration of ions in the region surrounding the pit was less in the presence of flow than under no-flow conditions. The decrease in ion concentration increased the resistivity of the

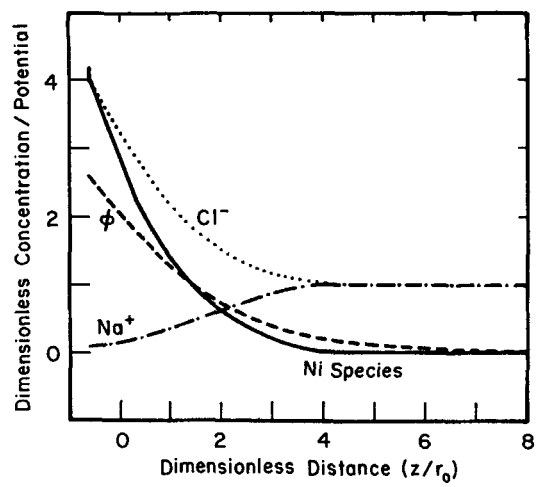

Figure 4. Variation of concentration and potential along the z-axis for $Pe = 10$, 1 M NaCl

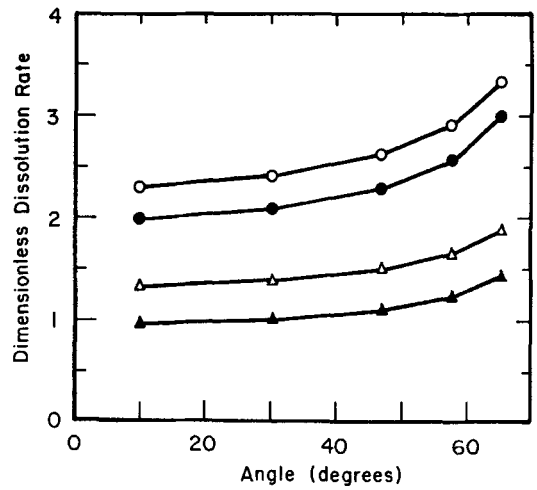

Figure 5. Variation of the local dissolution rate along the cavity surface (bottom, 0°; corner, 69°). 1·0 M NaCl: ○, $Pe = 0$; ●, $Pe = 500$. 0·25 M NaCl: △, $Pe = 0$; ▲, $Pe = 500$

solution in the cavity region. The increased resistance resulted in a greater potential drop in solution which decreased the percentage of the total applied potential available to drive the surface reaction. Since the total applied potential was constant for all runs, the result of increased flow was a lower dissolution rate as seen in Figure 5. A decrease in pit dissolution rate with increasing flow because of potential effects has also been observed experimentally.[5,10]

CONCLUSIONS

The commercial finite element code FIDAP has been modified in order to solve a new set of equations which include multiple species in solution, transport by migration and reaction

equilibria. The modified code was used to simulate the potential-dependent pitting of nickel in neutral salt solution. It was found that convective flow from an axisymmetric jet limited concentration variations to the region near the cavity. The flow, however, was not sufficient to cause the mass transfer boundary layer to penetrate the cavity mouth. The dissolution rate of the cavity decreased with increasing flow owing to an increase in the potential drop as the concentration of ions in the region surrounding the pit approached that of the bulk solution. The capabilities demonstrated in this paper represent a significant advancement in the modelling of pitting phenomena and a powerful tool for continuing research.

ACKNOWLEDGEMENTS

This work was funded by the Department of Energy, Office of Basic Energy Sciences via the Materials Research Laboratory at the University of Illinois at Urbana (ER1198). Fellowship support was received for J. N. Harb from the General Electric Foundation.

APPENDIX: NOMENCLATURE

c_i	concentration (gmol/cm^3)
$\mathbf{C}_i$	vector of nodal point concentrations (gmol/cm^3)
D_i	diffusivity (cm^2 s^{-1})
F	Faraday's constant (96500 C/*eq*)
i	species number
i_0	exchange current density (A cm^{-2})
K	equilibrium constant
N_i	molar flux (gmol/s cm^2)
$\mathbf{n}$	normal vector
Pe	Peclet number, $u_0 r_0/D$ (dimensionless)
r_0	radius of pit opening (cm)
R	dimensionless distance, r/r_0
T	absolute temperature (K)
u_i	ionic mobility (cm^2 gmol/J s)
u_0	characteristic velocity of cavity (cm s^{-1})
$\mathbf{v}$	velocity (cm s^{-1})
$\mathbf{V}$	dimensionless velocity, $\mathbf{v}/u_0$
$\mathbf{V}_b$	dimensionless velocity at outer boundary
Z	dimensionless distance, z/r_0
z_i	charge number (*eq*/gmol)

Greek letters

β	Tafel parameter (V^{-1})
ϕ	potential in solution (V)
$\boldsymbol{\phi}$	vector of nodal point potentials (V)
Γ	finite element shape functions

REFERENCES

1. M. Datta and D. Landolt, 'On the role of mass transport in high rate dissolution of iron and nickel in ECM electrolytes—I. chloride solutions', *Electrochem. Acta*, **25**, 1255 (1980).
2. M. Magini, G. Paschina and G. Piccaluga, 'Ni–Cl bonding in concentrated Ni(II) aqueous solutions at high Cl^-/Ni^{+2} ratios. An X-ray diffraction investigation', *J. Chem. Phys.*, **76**, 1116 (1982).

3. D. F. C. Morris, G. L. Reed, E. L. Short, D. N. Slater and D. N. Waters, 'Nickel (II) chloride complexes in aqueous solution', *J. Inorg. Chem.*, **27**, 377 (1965).
4. J. R. Galvele, 'Transport processes in passivity breakdown—II. full hydrolysis of the metal ions', *Corros. Sci.*, **21**, 551 (1981).
5. J. N. Harb, 'Experimental and theoretical investigation of pitting corrosion on nickel in chloride solution', *Ph.D. Thesis*, University of Illinois, Urbana, IL, 1988.
6. R. C. Alkire, D. B. Reiser and R. L. Sani, 'Effect of fluid flow on removal of dissolution products from small cavities', *J. Electrochem. Soc.*, **131**, 2795 (1984).
7. H. Schlichting, *Boundary-Layer Theory*, 7th edn, McGraw-Hill, New York, 1979, p. 100.
8. *FIDAP User's Manual*, Fluid Dynamics International, Inc., Evanston, IL, 1987.
9. R. L. Sani, P. M. Gresho, R. L. Lee and D. F. Griffiths, 'The cause and cure (?) of the spurious pressures generated by certain FEM solutions of the incompressible Navier–Stokes equations: parts I and II', *Int. j. numer. methods fluids*, **1**, 17 (1981).
10. T. Beck and S. G. Chan, 'Experimental observations and analysis of hydrodynamic effects on growth of small pHs', *Corrosion*, **37**, 665 (1981).